Transactions, **SMiRT-26**
Berlin/Potsdam, Germany, July 10-15, 2022
Division I

Development of a novel damage model for concrete accounting for creep, high temperature, and constraint effects

Jefri Draup[1†], Alexandre Gangnant[5], Graham Doughty[2], Jiansong Guo[2], Thomas Helfer[3], Giacomo Torelli[4]

[1] EDF Energy R&D UK Centre, Manchester, UK
[2] EDF Energy Nuclear Generation, East Kilbride, UK
[3] CEA, DEN, DEC, F-13108 Saint-Paul-Lez-Durance, France
[4] University of Sheffield, Sheffield, UK
[5] SIXENSE, NECS, Sceaux, France
[†]Corresponding author (jefri.draup@edfenergy.com)

Abstract

Concrete exhibits a complex range of visco-plastic behaviour over its temperature range. At room temperature, concrete demonstrates basic creep behaviour (without loss of mass) when supporting an external load. In response to thermal fluctuations, there is an additional component of creep linked to moisture content and its transport (drying creep). Furthermore, at high temperatures beyond a critical temperature and under an external load, concrete exhibits a component of plasticity referred to as load induced thermal strain (LITS) or transient thermal creep (TTC).

For pre-stressed concrete structures, the evolution of visco-plastic creep strains is important over the lifetime of a structure, with each component of strain playing a significant role under specific circumstances. For example, the evolution of LITS has the potential to induce both a loss in pre-stress and residual tensile stress development under transient thermal conditions. Hence, structures which have been subjected to a high temperature thermal loading cycle may experience cracking and subsequent loss of rigidity; this could ultimately lead to a loss of functionality or even structural failure. In contrast, the role of basic creep is more significant over the lifetime of structures, which in the nuclear industry is of the order of 50 years for operations, defuelling and decomissioning. Again, basic creep strains have the potential to contribute to cracking in structures.

Whilst models for basic and drying creep have been around for some time, models that capture LITS have only recently become available in the public domain. Furthermore, there are currently no available models that can capture cracking with plasticity that are accepted by industrial regulators as reliable. Most commercial software implement simple damage models, such as the model of Mazars (1986), but these cannot capture anisotropy and plasticity in addition to the unilateral effect exhibited by concrete. However, relatively recent research developments have shown that these additional effects can be captured using an energy regularisation method. For example, the Fichant-La Borderie (FLB) model is suitable to capture cracking due to plastic strains.

In this project a method for coupling inelastic strains, which originate from basic creep and LITS, with the FLB model is proposed. It is believed that this novel model will enable more accurate assessment of structural damage over the lifetime of structures, including during transient thermal events such as fires.

Introduction

The visco-plastic properties of concrete are complex and vary with temperature. Simply defined, creep is the time dependent deformation of a structure under sustained load. At room temperature, under load, concrete will exhibit instantaneous elastic strains and creep strains. The creep strain in concrete is composed of two basic elements: basic creep which occurs without loss of mass, and the additional drying creep which is linked to moisture content. The deformation of concrete in the absence of an applied load is often referred to as shrinkage (see Figure 30), as described by El Kanj et al. (2013).

The mechanisms of creep are thought to originate within the hardened cement paste and the failure of paste-aggregate bonds at high stresses, in an analogous way to dislocation motion in metals. Whilst the mechanisms are not fully understood, the diffusion of evaporable moisture within capillary pores of the cement paste can play a strong role in the strength and creep response of concrete, according to Bazant et al. (1982). This form of creep is deemed to be distinctly different from shrinkage, which is related to long term drying effects in concrete.

Various computational methods have also been developed that aimed to accurately represent creep and shrinkage. Bazant (2001) presents a detailed account of the various approaches in the public domain, but conclude that a comprehensive predictive model that captures all relevant mechanisms is very difficult. Nevertheless, it is noted that rate dependent creep models based on the Kelvin or Maxwell chains are highlighted as being able to give the most realistic representation of creep mechanisms as they allow physically sound incorporation of the effects of variable pore humidity and temperature on creep and aging.

At high temperatures and under mechanical constraint, experimental evidence indicates that concrete develops significant inelastic strains. According to a review by Torelli et al. (2016), this is known as load induced thermal strain (LITS). Whilst it is not fully understood, LITS is considered to have important role in the structural performance of concrete during loading at elevated temperatures. A numerical study by Torelli et al. (2018) indicated that LITS has the potential to contribute to loss in pre-tension in pre-stressed concrete strutures during transient loading.

Within the nuclear industry, the lifetime performance of structures is equally as important as transient behaviour; both are paramount to ensuring safe operations. Thus, there is an interest to understand the potential for damage to be caused by a range of mechanisms contributing to visco-plastic strain evolution in concrete, i.e. LITS and basic creep. It follows that accurate models that capture creep and LITS, which are also compatible with relevant damage models, could be helpful to assess this phenomena. Despite this need, numerical models that reliably capture the effects of visco-plastic strain components on damage evolution in concrete are not reliable for industrial usage. As noted by Draup et al. (2019) this can be linked to the domain of validity of damage models and the fact that typical concrete damage models were not developed with the explicit aim of capturing inelastic strain components.

Draup et al. (2019) proposed mathematical coupling between the Fichant-La Borderie damage model and a LITS model. This model was able to capture a range of properties of concrete, include: initial elastic properies; stiffness degradation due to micro-cracking; asymmetry between compressive and tensile behaviour; stiffness restoration due to crack closure or the unilateral effect; the evolution of LITS. Interestingly, the model was able to show that coupled behaviour models can better capture the complex evolution of strains under a range of conditions compared to standalone models. Most importantly, the coupled models are less

conservative than standalone models and can provide insight into the conditions affecting real structures. However, the coupled FLB-LITS damage model of Draup et al. can only be used to capture transient effects in concrete as it does not account for long term creep damage.

In this paper, a method for utilising the Burger creep model with the coupled FLB-LITS damage model is proposed. Preliminary results which demonstrate the complex evolution of stress, strain and damage within concrete are also presented. The constitutive behaviour laws are developed using the open source MFront software, which is a cross-platform constitutive modelling environment that is compatible with a range of commercial and open source finite element software, as described by Helfer et al. (2015).

Numerical modelling approach

A brief description of the modelling approach for Burger, LITS, FLB, and the finite element model setup utilised in this study are presented below.

LITS model

A confinement dependent model for LITS is discussed by Torelli et al. (2017); LITS is influenced to a stress triaxiality index. The rationale for this originates from a large body of experimental evidence, which shows that LITS as a dependency on stress confinement and is not simply a result of superposition of individual uniaxial stress states. However, the total strains are assumed to be composed as a sum of the elastic strains, free thermal strains, and the remainder being due to LITS, i.e.

$$\dot{\varepsilon}_{ij}^{lits} = \eta \frac{\beta(T)}{\sigma_{u0}} \left[-\nu_{lits} \sigma_{kk}^{-} \delta_{ij} + (1 - \nu_{lits}) \sigma_{ij}^{-} \right] \dot{T} \tag{1}$$

$$\eta = 1 + (C_m - 1)\gamma \tag{2}$$

$$C_m = \eta \frac{|\sigma_1^- + \sigma_2^- + \sigma_3^-|}{\sqrt{(\sigma_1^-)^2 + (\sigma_2^-)^2 + (\sigma_3^-)^2}} \tag{3}$$

$$\beta(T) = b_0 + b_1 T + b_2 T^2 + b_3 T^3 + b_4 T^4 \tag{4}$$

Equations 1-4 describe the confinement dependant LITS model, where η is the stress triaxiality function and γ is a material parameter that must be calibrated to experimental data for the appropriate temperature range. C_m is the stress triaxiality index and is linked to the principal stresses. *β(T)* is a polynomial function which is used to describe the experimentally observed uniaxial temperature-LITS behaviour from the public domain. σ_{u0} is the compressive strength of the material, σ_{ij}^{-} is the *(i,j)*th component of the stress tensor in the negative projection. Finally, υ_{lits} is a material parameter similar to the elastic Poisson's ratio.

FLB model

Gangnant et al. (2016) describe the FLB model, which is used to account for the inelastic sources of damage in concrete. Equation 5 is the damage scalar, which is based on classical damage mechanics with the added assumption that the stiffness decreases exponentially. Thus,

it is prohibited from reaching 0 allowing the avoidance of convergence issues. The strain component at the onset of damage is ε_{d0} whereas $\varepsilon_{eq}$is the equivalent inelastic (Equation 6). The unilateral effect of concrete, which is a partial stiffness restoration due to crack closure that was described by Ramtani (1990), is accounted for via Equation 7. B_t is the damage parameter which features an energy regularisation technique. Here f_t, G_t , and h are, respectively, the fracture tensile strength, fracture toughness, and element length. Finally, the the total stress tensor (Equation 8) is defined in terms of the damage scalar and the decomposed effective stress tensor, which is separated into the tensile and compressive parts to account for asymmetry. Here, α is a factor linked to damage in the compressive state.

$$D = 1 - \frac{\varepsilon_{d0}}{\varepsilon_{eq}} exp\{B_t(\varepsilon_{d0} - \varepsilon_{eq})\} \tag{5}$$

$$\varepsilon_{eq} = \sqrt{\sum_{i=1}^{3} \langle \varepsilon_i^e \rangle^2} \tag{6}$$

$$B_t = \frac{f_t h}{G_t - 0.5\varepsilon_{d0} h f_t} \tag{7}$$

$$\sigma_{ij} = (1 - D)\langle \tilde{\sigma}_{ij} \rangle_+ + (1 - D^\alpha)\langle \tilde{\sigma}_{ij} \rangle_- \tag{8}$$

Burger creep model

The basic components of the Burger creep model are: a Maxwell chain connected in series with a Kelvin (or Voigt) chain, as described by Bottoni (2018). The former is a spring and dashpot connected in series whilst the latter is a spring and dashpot connected in parallel.

The basic premise of the Burger creep model is that the creep strain can be decomposed into the recoverable (elastic) and irrecoverable (inelastic) components, which correspond to the spherical and deviatoric components of strain respectively (Equation 9). It follows that the stress tensor can be split in the corresponding spherical and deviatoric parts too (Equation 10), with contribution from the reversible (Equation 11-12) and irreversible components of strain (Equation 13-14).

$$\varepsilon_{cr} = \varepsilon_R^S + \varepsilon_I^S + \varepsilon_R^D + \varepsilon_I^D \tag{9}$$

$$\sigma = \sigma^S \bar{I} + \sigma^D \tag{10}$$

$$\sigma^S = k_R^S \times \varepsilon_R^S + \eta_R^S \times \dot{\varepsilon}_R^S \tag{11}$$

$$\sigma^D = k_R^D : \varepsilon_R^D + \eta_R^D : \dot{\varepsilon}_R^D \tag{12}$$

$$\sigma^S = \eta_I^S \times \dot{\varepsilon}_I^S \tag{13}$$

$$\sigma^D = \eta_I^D : \dot{\varepsilon}_I^D \tag{14}$$

Coupled Burger, LITS and FLB

In order to ensure the coupling between the individual models, the equivalent strain (Equation 6) in the FLB model needs to be adapted to account for the contribution to damage from creep strains (Equation 15).

$$\varepsilon_{eq} = \sqrt{\sum_{i=1}^{3} \langle \varepsilon_i^e \rangle_+^2 + \beta \langle \varepsilon_i^{cr} \rangle_+^2} \tag{15}$$

The coupling is essentially a sequential computation of the total strain made by evaluating the components contributing to the total strain in the following order:

1. Computation of creep strain.
2. Computation of damage
3. Computation of high temperature LITS

Firstly, the creep strain is evaluated using the Burger creep model, which allows extraction of the spherical and deviatoric components of both the irrecoverable and recoverable strains. The elastic strain tensor is computed and used alongside the creep strain tensor in order to compute an equivalent strain tensor; this requires an adaptation to the FLB damage model. The equivalent strain is then used to compute the damage scalar in the presence of creep strains using the adapted FLB damage model. Secondly, the damage scalar is then utilised to compute an effective stress in a damaged element. This effective stress can then be decomposed into the positive and negative parts in order to compute the LITS strain. Finally, the LITS behaviour law is evoked in order to compute the LITS component of the inelastic strains. Once all these components are computed, the final stress tensor can be updated.

Following the approach of Draup et al. (2019), the coupled inelastic Burger, FLB and thermoelastic LITS model are formulated to be integrated using an implicit θ-sheme. A priori, the unknowns to be solved are the increments of: the elastic strain $\Delta\varepsilon^{el}$; the creep strain $\Delta\varepsilon^{cr}$; the LITS strain $\Delta\varepsilon^{vp}$; damage Δd. As discussed here, the increment of damage Δd can be eliminated from this implicit system. Therefore, one has to define two tensorial equations, which are, respectively, associated with the elastic strain and the inelastic strain which the increments $\Delta\varepsilon^{el}$and $\Delta\varepsilon^{vp}$ must satisfy. Equations 16-19 define the implicit system of equations to be solved, where Δt is the time increment.

$$f_{\underline{\varepsilon}^{el}}\left(\Delta\underline{\varepsilon}^{el}, \Delta\underline{\varepsilon}^{vp}, \Delta\underline{\varepsilon}^{cr}\right) = 0 \tag{16}$$

$$f_{\underline{\varepsilon}^{vp}}\left(\Delta\underline{\varepsilon}^{el}, \Delta\underline{\varepsilon}^{vp}, \Delta\underline{\varepsilon}^{cr}\right) = 0 \tag{17}$$

$$f_{\underline{\varepsilon}^{el}} = \Delta\underline{\varepsilon}^{el} + \Delta\underline{\varepsilon}^{vp} + \Delta\underline{\varepsilon}^{cr} - \Delta\underline{\varepsilon}^{to} \tag{18}$$

$$f_{\underline{\varepsilon}^{vp}} = \Delta\underline{\varepsilon}^{vp} - \Delta\underline{\varepsilon}^{cr} - \Delta\underline{\varepsilon}^{vp} + \Delta t f_{LITS}\left(\underline{\sigma}\big|_{t+\theta\Delta t}\right) \tag{19}$$

The FLB damage model introduces an explicit relationship between the stress and the elastic strain $\Delta\underline{\varepsilon}^{el}$as well as the damage Δd through Equation 20-23. In FLB models, the damage evolution Δd can be explicitly computed as a function of the elastic strain increment $\Delta\underline{\varepsilon}^{el}$. This means that σ|t+θΔt can be written as a function of $\Delta\underline{\varepsilon}^{el}$only, defined by Equation 25

$$\underline{\sigma}\big|_{t+\theta\Delta t} = f_{FLB}\left(\underline{\varepsilon}^{el}\big|_{t+\theta\Delta t}, \underline{d}\big|_{t+\theta\Delta t}\right) \tag{20}$$

$$\underline{\varepsilon}^{el}\big|_{t+\theta\Delta t} = \underline{\varepsilon}^{el}\big|_{t} + \theta\,\Delta\underline{\varepsilon}^{el} \tag{21}$$

$$\underline{d}\big|_{t+\theta\Delta t} = \underline{d}\big|_{t} + \theta\,\Delta d \tag{22}$$

$$\underline{\sigma}\big|_{t+\theta\Delta t} = f_{FLB}\left(\underline{\varepsilon}^{el}\big|_{t+\theta\Delta t}, \underline{d}\big|_{t+\theta\Delta t}\left(\Delta\underline{\varepsilon}^{el}\right)\right) \tag{23}$$

$$J = \begin{pmatrix} \dfrac{\partial f_{\underline{\varepsilon}^{el}}}{\partial\Delta\underline{\varepsilon}^{el}} & \dfrac{\partial f_{\underline{\varepsilon}^{el}}}{\partial\Delta\underline{\varepsilon}^{vp}} \\ \dfrac{\partial f_{\underline{\varepsilon}^{vp}}}{\partial\Delta\underline{\varepsilon}^{el}} & \dfrac{\partial f_{\underline{\varepsilon}^{vp}}}{\partial\Delta\underline{\varepsilon}^{vp}} \end{pmatrix} \tag{24}$$

$$\begin{aligned} \frac{\partial f_{\underline{\varepsilon}^{el}}}{\partial\Delta\underline{\varepsilon}^{el}} &= -\Delta t\,\frac{df_{LITS}}{d\underline{\sigma}\big|_{t+\theta\Delta t}}.\frac{d\underline{\sigma}\big|_{t+\theta\Delta t}}{d\Delta\underline{\varepsilon}^{el}} \\ &= -\Delta t\,\frac{df_{LITS}}{d\underline{\sigma}\big|_{t+\theta\Delta t}}.\left(\frac{\partial\underline{\sigma}\big|_{t+\theta\Delta t}}{\partial\underline{\varepsilon}^{el}\big|_{t+\theta\Delta t}}\frac{d\underline{\varepsilon}^{el}\big|_{t+\theta\Delta t}}{d\Delta\underline{\varepsilon}^{el}} + \frac{\partial\underline{\sigma}\big|_{t+\theta\Delta t}}{\partial d|_{t+\theta\Delta t}}\frac{dd_{t+\theta\Delta t}}{d\underline{\varepsilon}^{el}\big|_{t+\theta\Delta t}}\frac{d\underline{\varepsilon}^{el}\big|_{t+\theta\Delta t}}{d\Delta\underline{\varepsilon}^{el}}\right) \\ &= -\theta\Delta t\,\frac{df_{LITS}}{d\underline{\sigma}\big|_{t+\theta\Delta t}}.\left(\frac{\partial\underline{\sigma}\big|_{t+\theta\Delta t}}{\partial\underline{\varepsilon}^{el}\big|_{t+\theta\Delta t}} + \frac{\partial\underline{\sigma}\big|_{t+\theta\Delta t}}{\partial d|_{t+\theta\Delta t}}\frac{dd_{t+\theta\Delta t}}{d\underline{\varepsilon}^{el}\big|_{t+\theta\Delta t}}\right) \end{aligned} \tag{25}$$

The implicit system here is solved by a standard Newton algorithm, which requires its Jacobian matrix, J, to be computed (defined by Equation 24). J can be decomposed by blocks, where $\frac{\partial f_{\underline{\varepsilon}^{el}}}{\partial\Delta\underline{\varepsilon}^{el}}$, $\frac{\partial f_{\underline{\varepsilon}^{el}}}{\partial\Delta\underline{\varepsilon}^{vp}}$, and $\frac{\partial f_{\underline{\varepsilon}^{vp}}}{\partial\Delta\underline{\varepsilon}^{el}}$ are the identity. Computation of $\frac{\partial f_{\underline{\varepsilon}^{vp}}}{\partial\Delta\underline{\varepsilon}^{vp}}$ is more demanding since the derivative of the eigentensors must be computed. A symbolic expression of $\frac{\partial f_{\underline{\varepsilon}^{vp}}}{\partial\Delta\underline{\varepsilon}^{vp}}$ is given by Equation 25, using the relation $\frac{d\underline{\varepsilon}^{el}|_{t+\theta\Delta t}}{d\Delta\underline{\varepsilon}^{el}} = \theta\underline{\boldsymbol{I}}$. Whilst MFront can provide all the tools to compute those partial derivatives, another strategy is to let be computed numerically $\frac{\partial f_{\underline{\varepsilon}^{vp}}}{\partial\Delta\underline{\varepsilon}^{vp}}$.

3D Cracked cube model

In this simple testcase, a cube with geometry $0.1 \times 0.1 \times 0.1$ mm is used. The cube features a square shaped crack, which is positioned at *Z=0.05*mm parallel to the *x-y* plane. The geometry is meshed with 250 hexahedral quadratic elements, as shown in Figure 1. The mesh is subjected to the following boundary conditions: nodes on the planes parallel to the *x-y* plane at *z=0* are assigned displacement conditions *dz=0*; nodes on the plane parallel to the z-*x* plane at y*=0* are assigned displacement conditions d*y=0*; nodes on the plane parallel to the *y-z* plane at *x=0* are assigned displacement conditions *dx=0*. Further the nodes on the plane parallel to the *x-y* plane at *z=0.1* are assigned prescribed displacement conditions as shown in Figure 2. All nodes of the mesh are assigned thermal boundary conditions as shown in Figure 3.

The simulation is run with four separate material constitutive models: pure elastic, thermoelastic LITS, coupled FLB-LITS, and coupled Burger-FLB-LITS. The boundary conditions are kept identical in all case, allowing the evolution of stress and strain to be evoked due to material properties alone.

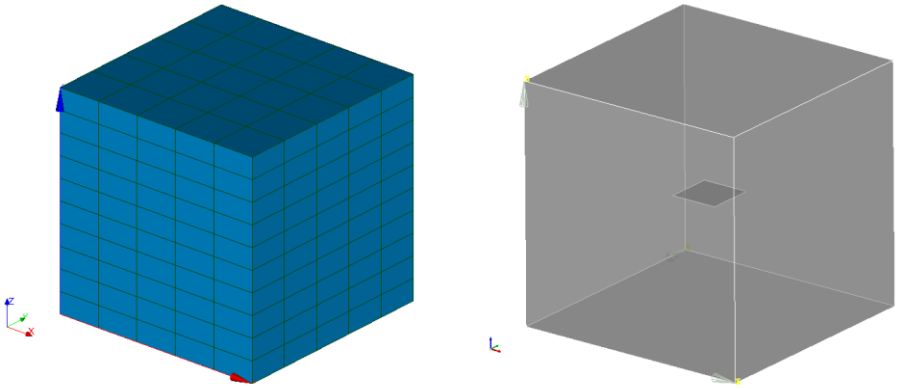

Figure 1 - mesh and geometry of specimen

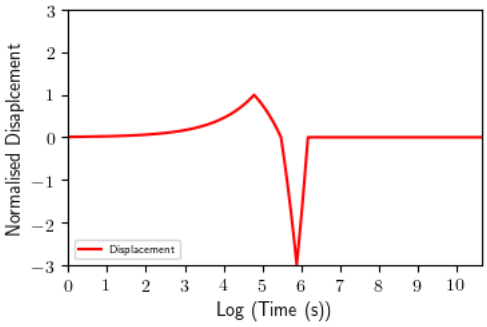

Figure 2 - Prescribed displacement boundary conditions

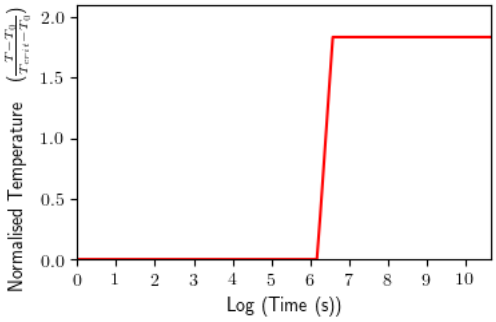

Figure 3 - Prescribed temperature boundary conditions

In this simple testcase, there are several phases to the loading:

- $t \leq 120$s : the cube undergoes tensile loading
- $120 < t \leq 240$s : the cube is unloaded
- $240 < t \leq 360$s : the cube undergoes compressive loading
- $360 < t \leq 480$s : the cube is unloaded
- $480 < t \leq 600$s : the cube undergoes restrained thermal expansion below the onset of LITS
- $600 < t \leq 720$s : the cube undergoes restrained thermal expansion above the onset of LITS
- $720 < t \leq 340$s : the cube is held at constant temperature and displacement conditions

These conditions are chosen to induce contributions to strain and damage evolution in the cube from various mechanisms, i.e. simple mechanical, LITS effects, and creep effects.

Results and Discussion

Figures 4-7 show the macro stress and displacement response of the cube when simulated using each of the material models. We take the elastic condition (Figure 4) as the baseline response. It is clear that each material model induces significant influence on the macro stress capacity of the cube. In particular, the evolution of LITS strains (Figure 5) causes a reduction of stress capacity due to stress relation. Further, the influence of damage in the coupled FLB-LITS model (Figure 6) causes a reduction of stress capacity compared to the LITS behaviour. Finally, the influence of creep strain evolution in the coupled Burger-FLB-LITS models (Figure 7) causes a time dependent reduction in stress capacity of the cube in comparison to the coupled FLB-LITS model.

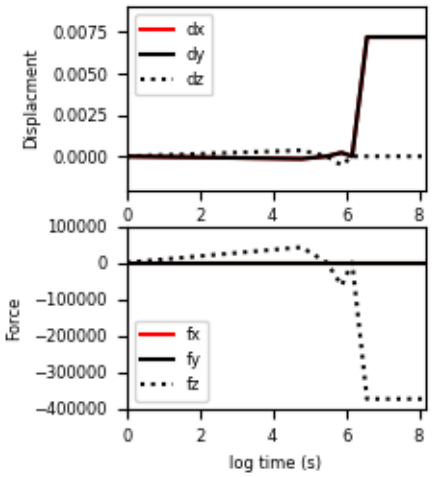

Figure 4 - Elastic response

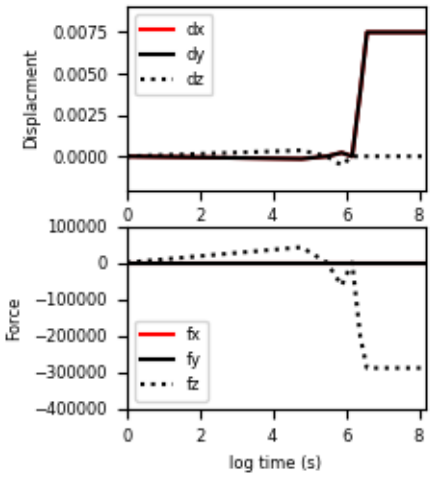

Figure 5 - LITS response

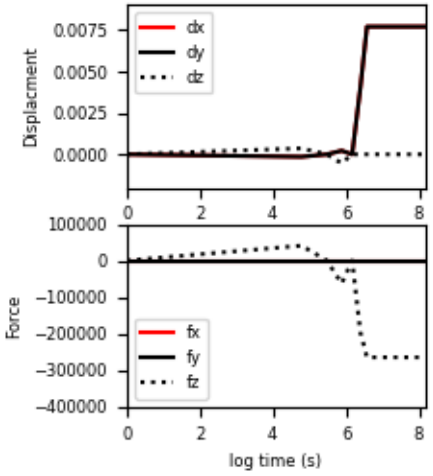

Figure 6 - coupled FLB-LITS response

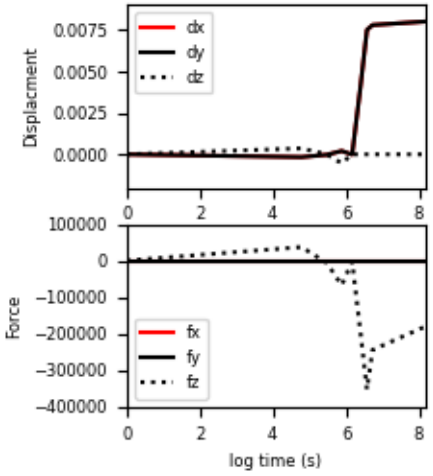

Figure 7 - coupled Burger-FLB-LITS response

Figure 8 shows the detailed comparison of stress fields in the cross section of the cube parallel to the *z-x* plane at *y=0.05*mm, which are shown at key points during the loading. Figure 9 shows the corresponding strain fields and Figure 10 shows the corresponding damage patterns.

The observation from Figure 8 is that stress fields evolve even during the low temperature loading regime during the tensile phase; this difference is observable at t=240s and is manifested as a residual compressive stress field. These differences can be traced to the evolution of creep strains (Figure 9). It should also be noted that the evolution of creep strains has the effect of reducing the damage levels that evolve under the tensile loading phase (Figure 10).

A similar effect can be seen from the compression phase, with an equally pronounced difference in residual stress fields at *t=480*s. It should be noted here that the distribution of damage here is different from the tensile phase, with damage occurring near the cracked interfaces. In the testcase we have presented, contact is neglected and this damage is likely to arise from bending of the cracked surfaces.

As the cube is loaded thermally, before the onset of LITS evolution, we see that the stress and strain fields are quite similar in all cases. This is likely due to the relatively large effect of thermal stresses compared to the mechanical loads for this particular case. We observe at *t=600*s similar stress, strain, and compressive damage patterns in the cube.

As the cube is loaded to higher temperature above the onset of LITS, we begin to see the reduction in stress capacity of the cube at *t=720*s. Interestingly, there is a significant change to the damage patterns when considering the influence of LITS and creep in combination. There is a greater absolute strain distribution in the cube due to the simultaneous evolution of creep and LITS.

As the cube is held at constant thermal and displacement conditions, at *t=3400*a, we see that the creep evolution has caused significant degradation to the stress capacity of the cube. What is interesting is that the creep strains have not caused much significant change to the damage distribution in the cube. This may be important when considering the effect of transient thermal loads on ageing infrastructure, i.e. for concrete structures with significant creep strain evolution.

It could be that the evolution of creep limits a structures potential for LITS evolution. This is because creep strains cause a reduction in stress capacity, and since LITS evolves under combined thermal loads and constraint, the evolution of LITS could be reduced in aged structures.

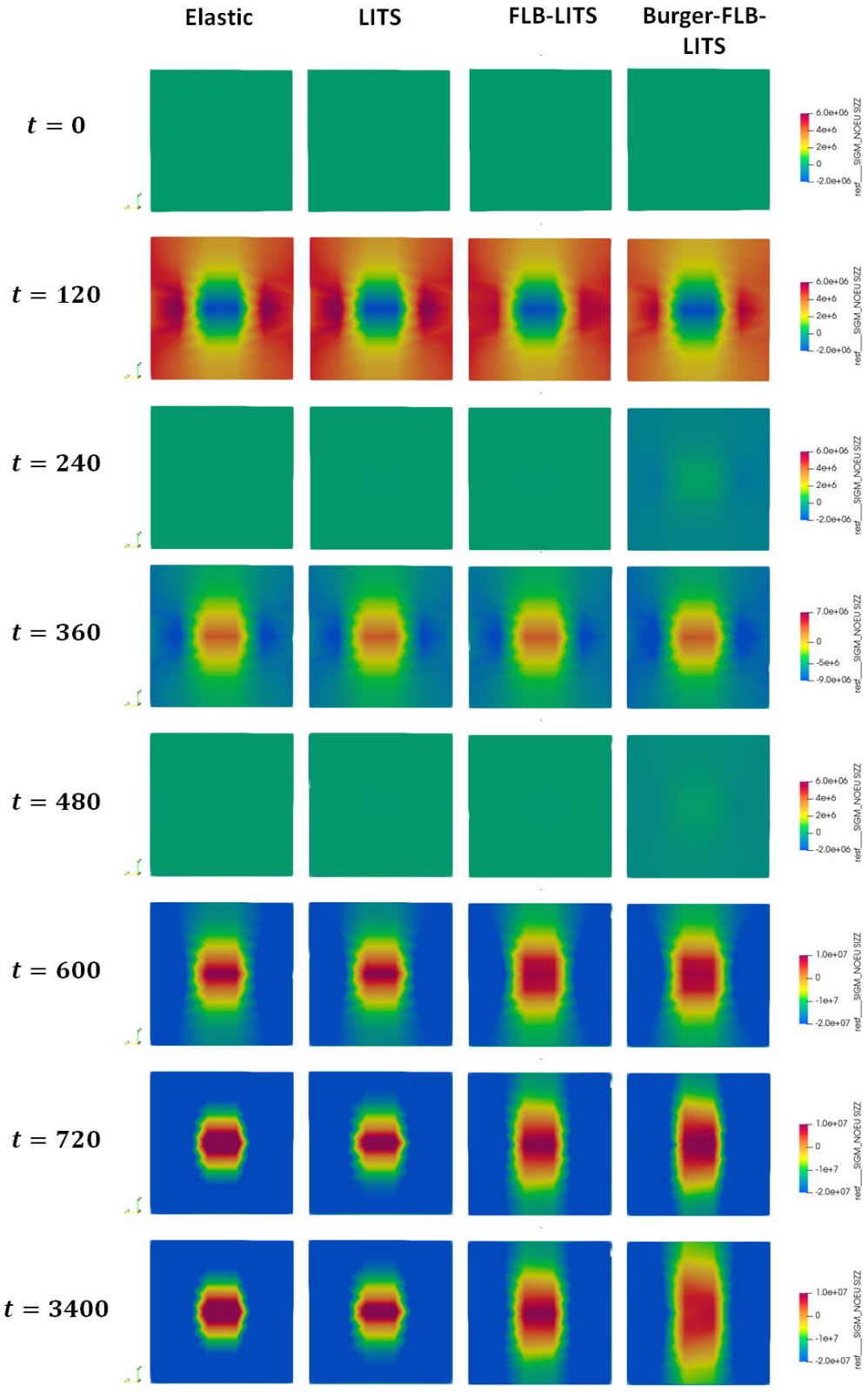

Figure 8 - Localised stress distribution

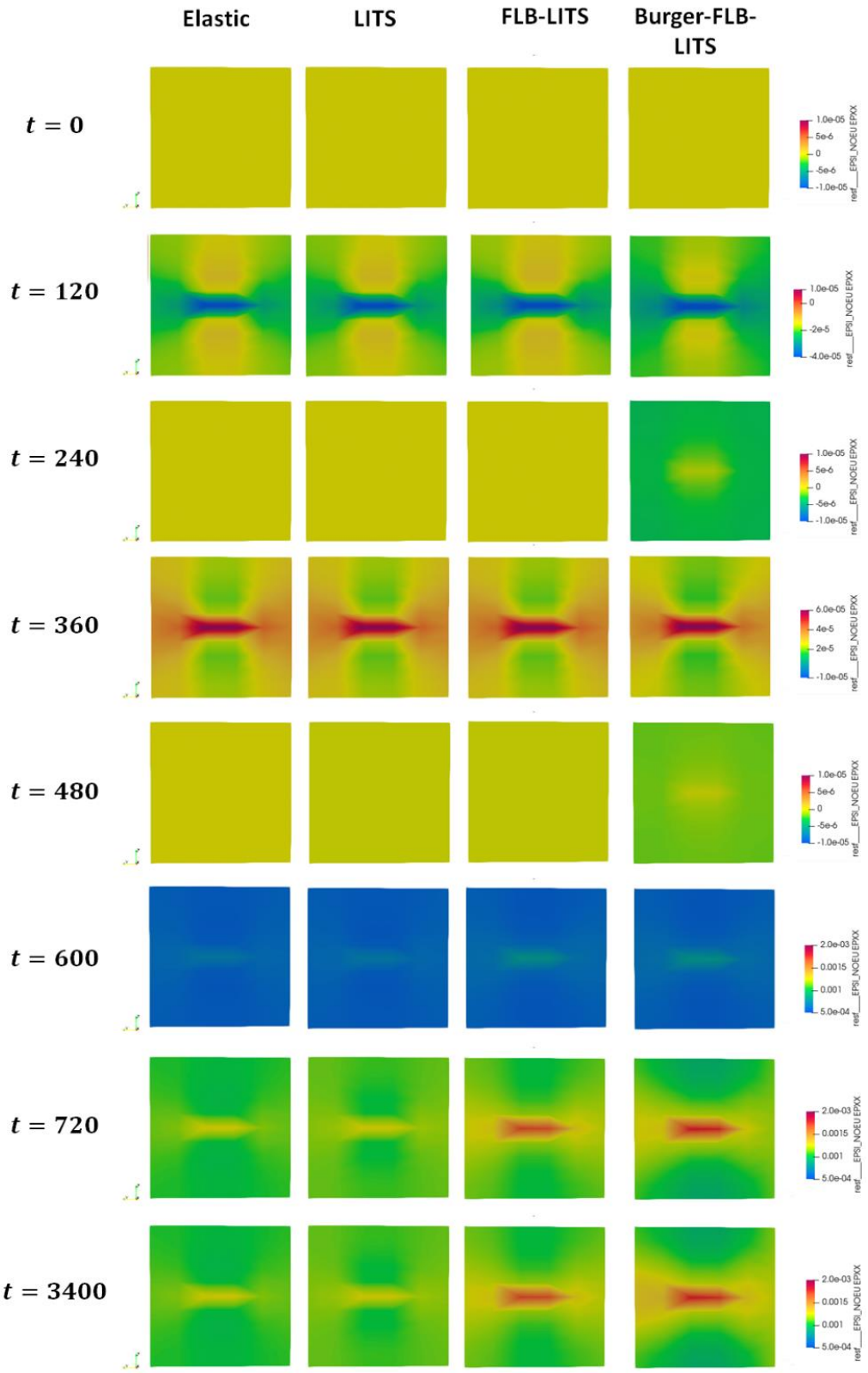

Figure 9 - Localised strain distribution

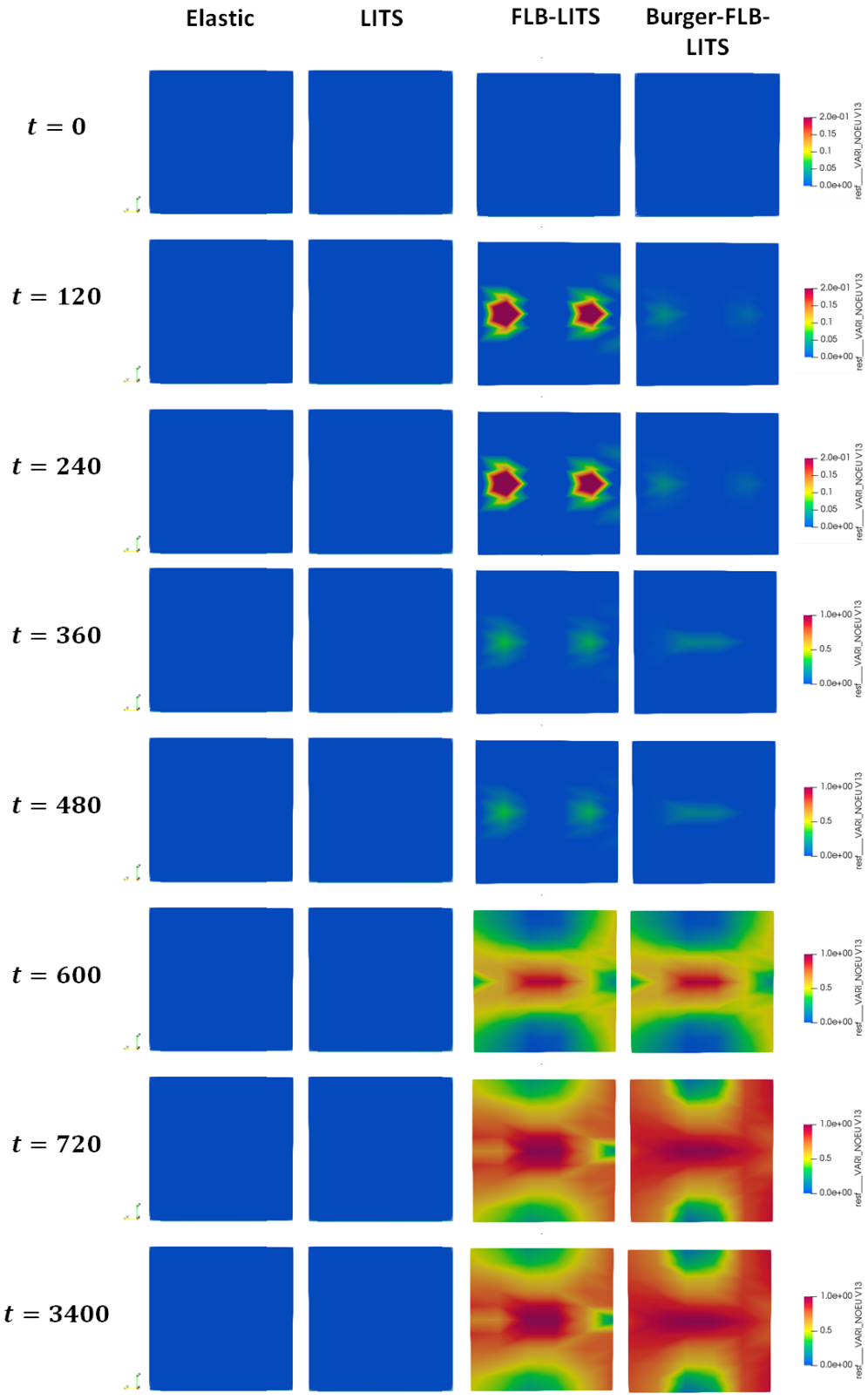

Figure 10 - Localised damage distribution

Conclusions

A novel model for concrete has been presented, which captures high temperature, constraint, and creep effects. The model is the result of a mathematically coupling between the Burger creep model, the FLB damage model, and a LITS model.

The model capability is showcased by running a simulation of a simple cube under thermal and mechanical constraints. The coupled Burger-FLB-LITS model is compared to the coupled FLB-LITS model of Draup et al. (2019), the thermos-elastic LITS model of Torelli et al. (2017), and a simple elastic model.

The comparisons show that markedly different macro response is produced when creep and LITS effects are taken into account. Moreover, it is possible that the creep strains can mitigate the evolution of LITS in concrete structures which are creep aged. This result indicates that the significance of LITS evolution on damage evolution during transient thermal events may not be as much as previously suggested in the public domain.

References

Torelli, G., Mandal, P., Gillie, M. and Tran, V.X. (2016). *"Concrete strains under transient thermal conditions: a state-of-the-art review,"* Engineering Structures, *127, 172-188*

Torelli, G., Gillie, M., Mandal, P. and Tran, V.X. (2017). *"A multiaxial load-induced thermal strain constitutive model for,"* International Journal of Solids and Structures, *108, 115-125*

Mazars, J. (1986). *"A description of micro- and macro scale damage of concrete structures,"* Engineering Fracture Mechanics, *25, 729-737*

Bazant, Z.P. (2001). *"Prediction of concrete creep and shrinkage: past, present and future."* Nuclear Engineering and Design, *203, 7-38*

Bazant, Z.P. and Whittmann, F.H. (1982). *"Creep shrinkage in concrete structures."* John Wiley & Sons.

Draup, J., Gangnant, A., Colette, G., Doughty, G., Guo, J., Helfer, T., Torelli, G., and Mandal, P. (2019*). "Development of a novel damage model for concrete subjected to high temperature and constraint,"* Proceedings of the SMiRT-25 conference.

Bottoni, M. (2018*). "R7.01.35: Relation de comportement BETON_BURGER pour le fluage du béton,"* code_aster documentation.

El Kanj, T. (2013*). "Modélisation du fluage propre du béton,"* PhD thesis, Université Libanaise.

Gangnant, A., Saliba, J., La Borderie, C., and Morel, S. (2016*). "Modeling of the quasibrittle fracture of concrete at meso-scale: Effect of classes of aggregates on global and local behavior,"* Cement and concrete research, *89, 35-44*

Ramtani, S. (1990). "*Contribution à la modélisation du comportement multiaxial du béton endommagé avec description du caractère unilateral*," Thesis, Paris 6. 9, 11, 35

Helfer, T., Michel, B., Proix, J.-M., Salvo, M., Sercombe, J., and Casella, M. (2015). "*Introducing the open-source mfront code generator: Application to mechanical behaviours and material knowledge management within the PLEIADES fuel element modelling platform*". 70(5):994–1023.